Collapse and revival dynamics of number-squeezed superfluids of ultracold atoms in optical lattices

E. Tiesinga

Joint Quantum Institute, National Institute of Standards and Technology and University of Maryland,
100 Bureau Drive, Stop 8423 Gaithersburg, Maryland 20899-8423, USA

P. R. Johnson

Department of Physics, American University, Washington DC 20016, USA

Recent experiments have shown a remarkable number of collapse-and-revival oscillations of the matter-wave coherence of ultracold atoms in optical lattices [Will *et al.*, Nature 465, 197 (2010)]. Using a mean-field approximation to the Bose-Hubbard model, we show that the visibility of collapse-and-revival interference patterns reveal number squeezing of the initial superfluid state. To describe the dynamics, we use an effective Hamiltonian that incorporates the intrinsic two-body and induced three-body interactions, and we analyze in detail the resulting complex pattern of collapse-and-revival frequencies generated by virtual transitions to higher bands, as a function of lattice parameters and mean-atom number. Our work shows that a combined analysis of both the multiband, non-stationary dynamics in the final deep lattice, and the number-squeezing of the initial superfluid state, explains important characteristics of optical lattice collapse-and-revival physics. Finally, by treating the two- and three-body interaction strengths, and the coefficients describing the initial superposition of number states, as free parameters in a fit to the experimental data it should be possible to go beyond some of the limitations of our model and obtain insight into the breakdown of the mean-field theory for the initial state or the role of nonperturbative effects in the final state dynamics.

I. INTRODUCTION

Optical lattices have become a powerful tool for studying the quantum many-body states of ultracold atoms [1, 2]. In 1998 Jaksch *et al.* [3] suggested using ultracold atoms in an optical lattice to simulate the Bose-Hubbard model [4], and in 2002 Greiner *et al.* [5] demonstrated Mott insulator quantum phase transitions by imaging atoms released from a lattice after a period of free expansion, which reveals the atomic momentum distribution at the moment of release. Recently, the *in-situ* measurement of the position of atoms has become possible [6–8], and techniques to measure higher-order correlation functions, thermodynamic properties such as pressure, temperature, and transport properties have been developed [9–11]. In the Mott state pairs of atoms have been studied spectroscopically [12–14].

In parallel, techniques have been developed to create and exploit the non-stationary dynamics of many-body states and their interactions. In collapse and revival experiments [15–17], a sudden increase in lattice depth projects an initial ground state into a non-equilibrium state which is held in the deep lattice for a variable period of time t. Coherence between confined atoms at the moment the lattice is switched off results in an interference pattern in the atom-density after a period of free expansion of the atom cloud [18]. The interaction-induced non-stationary dynamics in the lattice cause the degree of coherence to oscillate in time, which in turn makes the

visibility of imaged interference patterns, defined here as the ratio of atoms in interference peaks divided by the total number of atoms, to oscillate as a function of t.

In Ref. [19] we showed that the crucial role of multiband physics in collapse and revival dynamics can be elegantly described by extending the Bose-Hubbard model to include effective three- and higher-body interactions. After developing a new technique greatly reducing dephasing from inhomogeneities, Will *et al.* [17] recently observed tens of collapse-and-revival oscillations, which confirmed the predicted higher-body effects [19]. The experimental data had characteristics, however, not explained by higher-body interactions alone, and Will *et al.* [17] suggested that the data reveals additional information about the initial many-body state.

In this paper, we show that a combined analysis of both the number-squeezing of the initial superfluid state and the non-stationary multiband dynamics in the final deep lattice explains important characteristics of collapse-and-revival physics. First, we show how the visibility of the interference patterns depends on the degree of number-squeezing of the initial superfluid in the shallow lattice, providing a new tool for analyzing many-body states in optical lattices. Next, to describe the dynamics in the deep lattice, we use an effective Hamiltonian that incorporates the intrinsic two-body and induced three-body interactions, and we analyze in detail the resulting complex pattern of collapse-and-revival frequencies generated by virtual transitions to higher bands. In particular, we

show that the frequencies appearing the time evolution of the interference pattern visibilities are robust under changes in mean atom number, with number squeezing only affecting the spectral weights. Finally, by treating the two- and three-body interaction strengths, and the coefficients describing the initial superposition of number states, as free parameters in a fit to the experimental data it should be possible to go beyond some of the limitations of our model and obtain insight into the breakdown of the mean-field theory for the initial state or the role of nonperturbative effects in the final state dynamic

II. SHALLOW LATTICE AND INITIAL STATE

The initial state of atoms in an optical lattice is well described by the ground state of the three-dimensional (3D) Bose-Hubbard model with its parameters in a regime where tunneling cannot be neglected. The many-body ground state to good approximation factorizes into a product of single-site states [3]. The breakdown of the factorization for small lattices has been studied in [20].

In previous analyses of collapse-and-revival experiments [15–17], the single-site state was modeled as a coherent atom-number state $|\beta\rangle = e^{\beta b^\dagger - \beta^* b}|0\rangle$ with mean atom number $\langle n \rangle = \langle b^\dagger b \rangle = |\beta|^2$, where the operators b and $b^\dagger$ annihilate and create atoms in a lattice site, respectively, and $|0\rangle$ is the zero atom vacuum. This model captures basic aspects of the physics, but predicts contrasts and spectral weights of the interference visibilities that differ significantly from the data (e.g. compare the theoretical predictions in [19] to the data in [17]). For example, the data in [17] show minimal visibilities that are no smaller than 40% for some system parameters, before dephasing from inhomogeneities is significant, which is much larger than the minimum visibility $e^{-4\langle n \rangle}$ predicted for collapse of a coherent state.

Below, we show that these deviations are associated with the number squeezing predicted by a mean-field decoupling approximation [21, 22]. This approximation gives the Hamiltonian for each lattice site

$$H_i = -zJ_i\phi(b + b^\dagger) + zJ_i\phi^2 + \frac{1}{2}U_{2,i}\, b^\dagger b^\dagger bb - \mu\, b^\dagger b\,, \quad (1)$$

where $z = 6$ is the number of nearest-neighbor sites in the 3D lattice, J_i is the tunneling parameter, $U_{2,i}$ is the on-site atom-atom interaction strength, and μ is the chemical potential, which sets the mean atom number. The ground state is the lowest eigenstate of the non-number conserving H_i corresponding to a real-valued ϕ that minimizes the energy. For this value of ϕ the superfluid order parameter $\langle b \rangle = \phi$. A zero value for ϕ implies a Mott state with definite atom number per lattice site. Reference [23] describes the breakdown of this approximation for 1D and 2D systems.

Explicit expressions for J_i and $U_{2,i}$ (see [22]) contain overlap integrals of Wannier functions with the single-atom Hamiltonian and the atom-atom interaction poten-
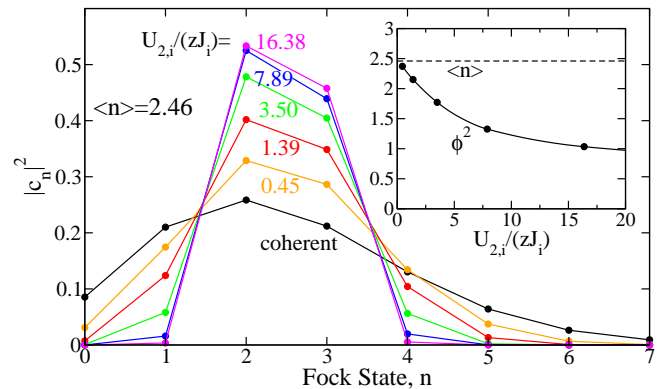

FIG. 1: (Color online) The probabilities $|c_n|^2$ for atom-number states $|n\rangle$ at each lattice site calculated from a mean-field decoupling approximation to the Bose-Hubbard model for several $\xi = U_{2,i}/(zJ_i)$ and fixed $\langle n \rangle = 2.46$. The curve labeled "coherent" corresponds to a coherent state with mean atom number $\langle n \rangle$. The inset shows the square of the order parameter as a function of ξ. The values of ξ corresponds to a linear increase of the lattice depth from $3E_R$ to $11E_R$ assuming ^{87}Rb atoms and laser wavelength of 738 nm. Here, E_R is the single-photon recoil energy of a ^{87}Rb atom.

tial, respectively. We consider lattices where the Wannier functions can be approximated by harmonic oscillator solutions, and assume a regularized 3D delta function potential for the two-body interactions between atoms [24] with a strength proportional to the scattering length of atoms colliding with zero relative kinetic energy [25]. These approximations allow us to obtain useful analytic results, although fully quantitative modeling should include the important role of the lattice anharmonicity.

To obtain the ground state for different initial lattice depths we numerically solve for the ground state of H_i using the variational solution $|\Psi_i\rangle = \sum_n c_n|n\rangle$, with Fock states $|n\rangle$ containing $n = 0, 1, 2, \cdots$ atoms and amplitudes c_n. We included n up to 20. Figure 1 shows examples of probabilities $|c_n|^2$ for Fock state components $|n\rangle$ of the ground state for several ratios of $\xi = U_{2,i}/(zJ_i)$, but fixed $\langle n \rangle$. The probabilities for a coherent state $|\beta\rangle$ with the same mean atom number are also shown. The ground state is number squeezed with increasing ξ, and for large ξ the Fock states closest to $\langle n \rangle$ dominate. In the opposite limit $\xi \to 0$ it approaches a coherent state, however, number-squeezing is readily apparent even for a shallow lattice as long as ξ is large enough that a single well-defined band exists. The inset shows the superfluid order parameter versus ξ. For small ξ the parameter ϕ approaches $\sqrt{\langle n \rangle}$, while for large ξ the order parameter slowly approaches zero. We next analyze how the frequencies and visibilities of the collapse and revival oscillations depend on the amplitudes c_n.

III.   EFFECTIVE DEEP LATTICE DYNAMICS

Collapse and revival dynamics start after a sudden increase in lattice depth, reducing the tunneling parameter to near zero. This operation is fast enough that interactions can be neglected but slow enough to prevent vibrational excitation in a lattice site. The state immediately after the lattice transformation retains the form $\sum_n c_n |n\rangle$, although the single particle basis functions change form slightly. Even with minimal real single-particle excitation, however, multiband effects are critical due to collision-induced virtual excitations to vibrationally-excited levels. We have shown that these effects can be concisely included via the effective Hamiltonian [19]

$$H_f = \frac{1}{2} U_{2,f} a^\dagger a^\dagger a a + \frac{1}{6} U_{3,f} a^\dagger a^\dagger a^\dagger a a a + \mathcal{O}\left(U_{2,f}^3\right) , \quad (2)$$

where $a^\dagger (a)$ creates (annihilates) an atom in a single renormalized spatial mode in a site of the final optical lattice and $U_{2,f}$ and $U_{3,f}$ give the strength of effective two- and three-body interactions.

The effective Hamiltonian H_f applies to deep lattices with no tunneling, such that the dynamics in each site is independent. This is valid for the experiments in [15–17], where the tunneling and three-body recombination rates are 1-2 orders of magnitude smaller than the three-body interaction strength. Recently, Ref. [26] showed ways to measure tunneling rates from collapse and revival experiments in less deep lattices. Effective three-body interactions have also been shown to govern thermalization of a one-dimensional Bose gas [27], and are important in Efimov physics [28].

Renormalization fixes the value of $U_{2,f}$ to the measured energy of two atoms held in a lattice site after the zero-point energy of two non-interacting atoms is subtracted (Alternately, Ref. [29] gives the exact analytical relationship between $U_{2,f}$ and the coupling constant of the regularized 3D delta function potential for two harmonically trapped atoms.) After renormalization, the effective three- and higher-body interactions are predicted in terms of $U_{2,f}$. Ignoring anharmonicities and assuming a harmonic potential with frequency ω_f, we showed in Ref. [19] that to second-order $U_{3,f}$ is attractive and given by

$$U_{3,f} = -c_f \, U_{2,f}^2 / (\hbar \omega_f), \quad (3)$$

with $c_f = 4\sqrt{3} + 6 \ln(4/(2+\sqrt{3})) - 6 = 1.344....$ The corrections due to anharmonicities in the deep lattices considered here are less than 5%.

The state evolves under H_f for hold time t. Since H_f is number conserving, the state becomes $|\Psi_f(t)\rangle = \sum_n c_n e^{-iE_n t/\hbar} |n\rangle$, where

$$E_n = U_{2,f} n(n-1)/2 + U_{3,f} n(n-1)(n-2)/6 \quad (4)$$

and $h = 2\pi\hbar$ is Planck's constant.

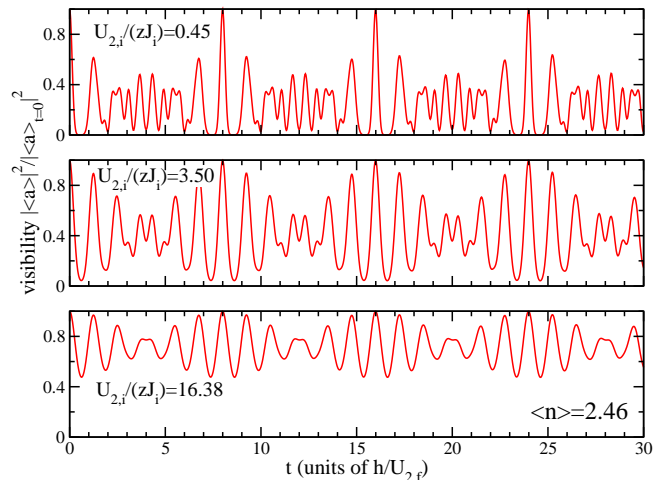
FIG. 2: (Color online) Visibility $|\langle a\rangle|^2/|\langle a\rangle_{t=0}|^2$ as a function of hold time t after a sudden increase of lattice depth. The three panels correspond to three initial states characterized by the ratio $\xi = U_{2,i}/(zJ_i)$ before the increase. The mean atom number is $\langle n\rangle = 2.46$ and the (renormalized) pair-wise interaction strength $U_{2,f} = 0.0928\hbar\omega_f$ for all traces. Time is in units of $h/U_{2,f}$ (e.g., 0.2 ms for ^{87}Rb in a 41 E_R deep lattice.)

IV.   INTERFERENCE PATTERNS

After hold time t, the optical lattice is turned off and the atoms freely expand. The visibility of the spatial interference pattern versus t yields information about both the initial state $|\Psi_i\rangle$ and the dynamics. In [15] it was shown that the visibility is $|\langle a\rangle|^2/|\langle a\rangle_{t=0}|^2 = |\langle a\rangle|^2/\phi^2$, where the expectation value is over $|\Psi_f(t)\rangle$. A zero visibility corresponds to a Gaussian spatial density profile, while a value of one corresponds to a diffraction pattern with maximum contrast.

Figure 2 shows time traces of the visibility versus t for three initial states differing in the value of $\xi = U_{2,i}/(zJ_i)$, and $\langle n\rangle = 2.46$ as in Fig. 1. The value $U_{2,f} = 0.0928\hbar\omega_f$ is typical for experiments with ^{87}Rb atoms in "deep" optical lattices. The traces show fast oscillations with timescale $\sim h/U_{2,f}$, and a slower envelope with a timescale $\sim h/U_{3,f}$. The pattern is more complex for initial states close to an ideal coherent superfluid, and there are near total collapses of the matter-wave coherence at regular intervals. For increasing ξ the initial state is increasingly number squeezed, and the traces become smoother. In qualitative agreement with the data in [17], there are only partial collapses of the visibilities.

The value for $\langle n\rangle$ is chosen to accentuate the effect of both two- and three-body interactions and corresponds to easily obtained experimental parameters. For smaller $\langle n\rangle$ we find that the contrast and three-body effects are reduced, while for larger $\langle n\rangle$ the effective Hamiltonian needs to be improved.

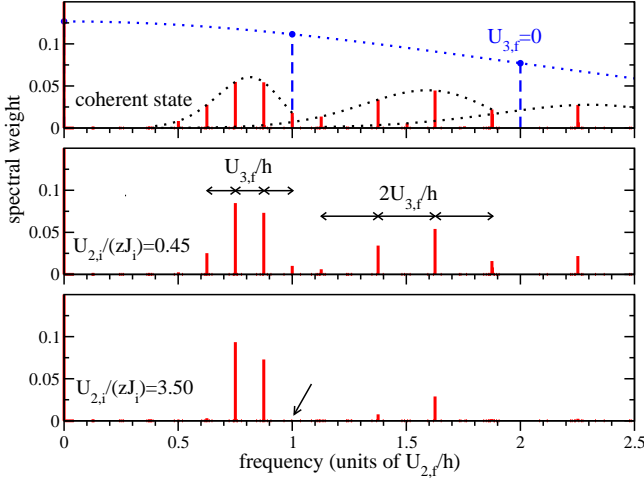The behavior of the visibility in Fig. 2 can be eluci-

FIG. 3: (Color online) Spectrum of visibility as function of positive frequency ν for initial coherent state (top panel) and two initial states obtained using mean-field decoupling approximation (bottom two panels). Time traces of the latter two spectra are shown in Fig. 2. We use $\langle n \rangle = 2.46$ and $U_{2,f} = 0.0928\hbar\omega_f$. Spectral lines correspond to the vertical lines. The spacings between dominant lines are shown in middle panel. The $\nu = 0$ line strength increases from 0.2 to 0.3 from the top to bottom panel. The arrow in the bottom panel shows the vanishing of a line at $h\nu = U_{2,f}$ for large ratio $U_{2,i}/(zJ_i)$. For coherent states, the spectrum with and without effective three-body interaction are shown as full and dashed lines, respectively. For $U_{3,f} = 0$ only frequencies with integer multiples of $U_{2,f}/h$ have nonzero line strength. The dotted curves are analytical expressions for the line strength, discussed in the text.

dated by performing a Fourier expansion. The allowed frequencies ν are differences between frequencies E_n/h governing the evolution of $|\Psi_f(t)\rangle$ [17]. Spectra of the visibility are shown in Fig. 3. The top panel shows the spectrum for an initial, ideal coherent state, while the bottom two panels show spectra for states calculated with the decoupling approximation. Consistent with the smoother traces in Fig. 2, fewer features are visible when ξ increases. For example, the arrow in the bottom panel of Fig. 3 highlights the disappearance of the line at $U_{2,f}/h$. This behavior is not obvious from examination of H_f alone and dramatically illustrates why the analysis presented here of the dynamics plus initial state is required to fully understand collapse and revival spectra.

The frequency components of $|\langle a \rangle|^2$ follow a regular pattern, yielding a method for obtaining the two- and three-body coupling strengths from the dynamics. A progression of equally spaced frequencies ends on or near each of the limits $kU_{2,f}/h$ for positive integer k. For example, for $\nu \le U_{2,f}/h$ features appear at

$$U_{2,f}/h + mU_{3,f}/h, \qquad (5)$$

for $m = 0, 1, 2, \cdots$. In fact, for $\nu \le kU_{2,f}/h$ and $k \ge 1$ the progression is $kU_{2,f}/h + (mk + k(k-1)/2)U_{3,f}/h$ for

$m = 0, 1, 2, \cdots$ corresponding to spacings between lines of $kU_{3,f}/h$. There are no lines at frequencies $kU_{2,f}/h$ except for $k = 1$.

The Fock state amplitudes c_n of the initial state $|\Psi_i\rangle$ can, in turn, be directly obtained from the line strengths. For example, the lines at $U_{2,f}/h + mU_{3,f}/h$ have a strength of $\sqrt{(m+2)(m+1)}|c_{m+2}^* c_{m+1}^2 c_m^*|/\phi^2$ (the expansion was previously shown in Ref. [17]), which depends on amplitudes of three Fock states. Again illustrating that complete analysis of the spectra is subtle, we note that for $m = 0$ the strength of the $U_{2,f}/h$ spectral line is proportional to c_0, the amplitude in the zero atom state! For example, for coherent or small ξ initial states the zero atom component has significant population (see Fig. 1) and the line at $U_{2,f}/h$ is visible; while for large ξ it disappears. The variations in line strength therefore correspond to the degree of superfluidity or number squeezing in the initial lattice state.

For coherent states, closed-form expressions for the line strengths may be obtained allowing a detailed comparison between the collapse-and-revival spectra for coherent and more realistic squeezed states. For a coherent state and $U_{3,f} = 0$, the visibility is $e^{2\phi^2(\cos(U_{2,f}t/\hbar)-1)}$ [17], which in the frequency domain implies lines at $kU_{2,f}/h$ for integer k with strength $e^{-2\phi^2}I_k(2\phi^2)$, where $I_k(z)$ is a modified Bessel function. This spectrum is shown in the top panel of Fig. 3, where the dotted curve connecting the blue vertical lines is found by replacing the integer order k of the Bessel function by $h\nu/U_{2,f}$.

The spectrum for an initial coherent state with $U_{3,f} \ne 0$ can also be solved analytically. Frequencies $U_{2,f}/h + mU_{3,f}/h$ have line strengths

$$\phi^2 e^{-2\phi^2}\phi^{4m}/(\Gamma(m+2)\Gamma(m+1)), \qquad (6)$$

and frequencies $2U_{2,f}/h + (2m+1)U_{3,f}/h$ have line strengths

$$\phi^4 e^{-2\phi^2}\phi^{4m}/(\Gamma(m+3)\Gamma(m+1)), \qquad (7)$$

where $\Gamma(z)$ is the Gamma function. Expressions for frequencies below $kU_{2,f}/h$ for $k > 2$ can also be found. This spectrum is shown in the top panel of Fig. 3, where the dotted curve connecting the lines is found by replacing m by the associated function of ν. For frequencies below U_2/h only lines near $U_{2,f}/h + \langle n \rangle U_{3,f}/h$ survive and, similarly, only frequencies near $2U_{2,f}/h + (2\langle n \rangle + 1)U_{3,f}/h$ survive.

We now study the dependence of the collapse and revival experiments on initial mean atom number, or equivalently the chemical potential. Figure 4 shows the visibility as a function of hold time for several initial values of mean atom number. The system parameters J_i and $U_{2,i}$ are held fixed and chosen such that the initial superfluid state shows significant squeezing. In contrast with Fig. 2 where the patterns change dramatically with ξ, Fig. 4 shows oscillation patterns that are robust to changes in mean atom number. This robustness is because the frequencies in the time-traces do not depend on the average
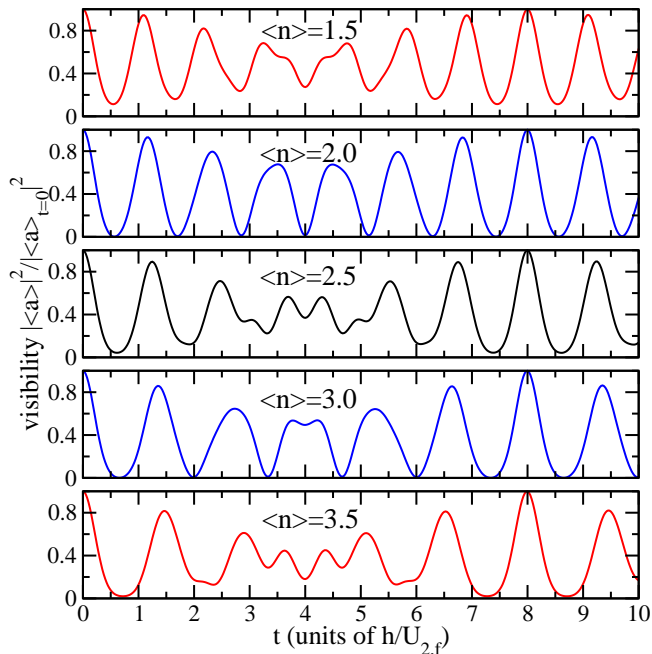
FIG. 4: (Color Online) Visibility as a function of hold time for initial states with a mean atom number $\langle n \rangle$ of 1.5, 2.0, 2.5, 3.0, and 3.5 going from the top to bottom panel. We use $\xi = U_{2,i}/(zJ_i) = 3.50$ and $U_{2,f} = 0.0928\hbar\omega_f$. The initial number probability and time trace for $\langle n \rangle = 2.5$ closely resembles that for $\langle n \rangle = 2.46$ and $\xi = 3.50$ shown in Figs. 1 and 2, respectively.

atom number, at least in the regime where the effective Hamiltonian H_f is valid. For example, the fast oscillations related to $h/U_{2,f}$ are in phase and the contrast is nearly independent of $\langle n \rangle$. This behavior can be understood from our analysis of the frequency components, which are independent of c_n and thus also mean-atom number. (For example, for $\nu \leq U_{2,f}/h$ spectral lines appear at $U_{2,f}/h + mU_{3,f}/h$ for $m = 0, 1, 2, \cdots$.)

In Fig. 4 the differences in the time evolution are only noticeable at half integer multiples of $h/U_{3,f}$, corresponding to $t \approx 4.0h/U_{2,f}$ in the figure. At these times the contribution to the phase factor $e^{-iE_n t/\hbar}$ appearing in the evolution of $|\Psi_f(t)\rangle$ due to the three-body interaction is -1 for the $n = 3, 7, 11, ...$ Fock states $|n\rangle$.

V. MEAN ATOM-NUMBER UNCERTAINTIES

We can quantify possible dephasing effects due to experimental uncertainties in preparing the superfluid with the same mean atom number $\langle n \rangle$ or equivalently the same chemical potential. An experimental sequence requires a new preparation of the superfluid for each hold time as the measurement of the interference pattern is destructive. We model this uncertainty by introducing a proba-

bility distribution $p(\langle n \rangle)$ over $\langle n \rangle$ and calculate

$$\rho(t) = \int_0^\infty d\langle n \rangle \, p(\langle n \rangle) \, |\langle a \rangle|^2 \,, \tag{8}$$

which is time dependent through $\langle a \rangle$. The visibility becomes $\rho(t)/\rho(0)$. Figure 5 shows time traces of the visibility after averaging over a Gaussian distributed $p(\langle n \rangle)$ normalized to one for $\langle n \rangle \geq 0$. The three curves correspond to Gaussian distributions centered at an average of 2.46 atoms, and with a square root of the variance (standard deviation) that is either zero, 10%, or 20% of the average value, respectively. As in Fig. 4 we immediately note that the revivals occur at the same times with only small changes in amplitude, demonstrating that collapse and revival experiments are robust under small variations in mean-atom number. A consequence of this independence is that in the frequency domain there is no broadening of the spectral lines due to uncertainties in the mean atom number after averaging over experimental realizations. There is broadening due to other mechanisms. For example, inhomogeneities leading to a variation of $U_{2,f}$ across the lattice, as well as thermal effects, will cause both broadening and dephasing. The successes of the experiments in Ref. [17] are made possible by the ability to reduce these effects sufficiently to allow observation of tens of oscillations.
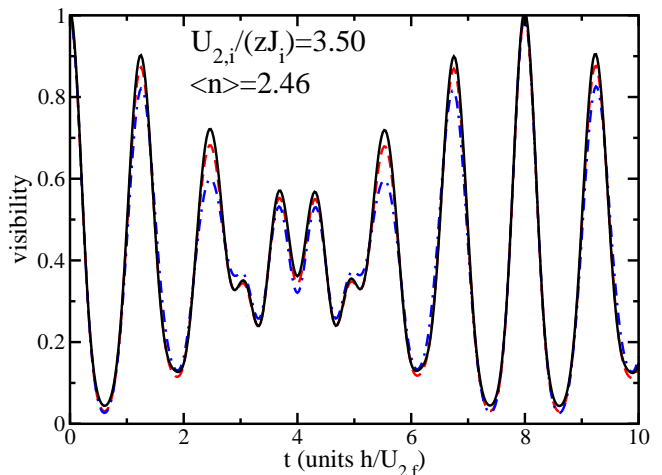

FIG. 5: (Color online) Visibility as a function of hold time for three different averages over an experimental uncertainty in initial mean-atom number (or equivalently chemical potential) in the superfluid. We use $\xi = U_{2,i}/(zJ_i) = 3.50$ and $U_{2,f} = 0.0928\hbar\omega_f$. The full (black) curve, already shown in Fig. 2, assumes complete reproducibility at $\langle n \rangle = 2.46$, while the dashed (red) curve use a Gaussian distribution with a mean atom number of 2.46 and a standard deviation equal to 0.25 (or relative uncertainty of 10%). The dash-dotted (blue) curve is obtained for a standard deviation of 0.5 (or relative uncertainty of 20%).

VI. CONCLUSIONS

We have shown that collapse-and-revival dynamics of atoms in optical lattices are strongly sensitive to both the initial many-body ground state and effective higher-body dynamics when projected into a deep lattice. The spectral analysis of the time evolution gives detailed information about effective interaction strengths as well as amplitudes of atom-number states superposed in the initial state. For example, number squeezing is apparent in the bottom two panels of Fig. 3, where fewer frequency components are present than for the coherent state shown in the top panel. We also found that the frequencies follow regular patterns that are independent of the initial superposition of number states, and the line strengths give information about the initial state.

Our analysis is based on various approximations. Future work should evaluate corrections to the decoupling approximation for small lattice depths. For example, Ref. [23] showed a marked effect of dimensionality on the Mott phase transition, and Ref. [26] analyzed the role of tunneling in collapse and revival dynamics. Finite temperature effects may also be important. Wedding-cake structures [3] that occur with additional weak confinement can be included using a local-density approximation. Three-body recombination should be included in the analysis when in the future the dynamics are studied over a longer period of time than currently observed. The inclusion of the anharmonicity of the lattice-site potential, which reduces the level spacing and affects the relationship between the effective two- and three-body interaction, can be taken into account to construct an improved theoretical model.

Despite these technical limitations, however, the combination of effects considered here captures important features of the collapse-and-revival dynamics. By treating the interaction strengths $U_{2,f}$ and $U_{3,f}$, and the initial state coefficients c_n, as free parameters in a fit to the experimental data it should be possible to both test our model, and correct for some of its limitations, for example, the neglect of the effects of anharmonicities. Inconsistencies in the fit could then provide insight into the breakdown of the mean-field theory (including thermal effects) for the initial state or the role of nonperturbative effects in the final state dynamics.

[1] O. Morsch and M. Oberthaler, Rev. Mod. Phys. **78**, 179 (2006).

[2] I. Bloch, J. Dalibard, and W. Zwerger, Rev. Mod. Phys. **80**, 885 (2008).

[3] D. Jaksch, C. Bruder, J. I. Cirac, C. W. Gardiner, and P. Zoller, Phys. Rev. Lett. **81**, 3108 (1998).

[4] M. P. A. Fisher, P. B. Weichman, G. Grinstein, and D. S. Fisher, Phys. Rev. B **40**, 546 (1989).

[5] M. Greiner, O. Mandel, T. Esslinger, T. W. Hänsch, and I. Bloch, Nature **415**, 39 (2002).

[6] K. D. Nelson, X. Li, and D. S. Weiss, Nat. Phys. **3**, 556 (2007).

[7] N. Gemelke, X. Zhang, C. Hung, and C. Chin, Nature **460**, 995 (2009).

[8] W. S. Bakr, A. Peng, M. E. Tai, R. Ma, J. Simon, J. I. Gillen, S. Flling, L. Pollet, and M. Greiner, Science **329**, 547 (2010).

[9] R. Jordens, N. Strohmaier, K. Gunter, H. Moritz, and T. Esslinger, Nature **455**, 204 (2008).

[10] C. Hung, X. Zhang, N. Gemelke, and C. Chin, Phys. Rev. Lett. **104**, 160403 (2010).

[11] T. Ho and Q. Zhou, Nat. Phys. **6**, 131 (2010).

[12] H. Moritz, T. Stöferle, K. Günter, M. Köhl, and T. Esslinger, Phys. Rev. Lett. **94**, 210401 (2005).

[13] C. Ospelkaus, S. Ospelkaus, L. Humbert, P. Ernst, K. Sengstock, and K. Bongs, Phys. Rev. Lett. **97**, 120402 (2006).

[14] A. Widera, F. Gerbier, S. Fölling, T. Gericke, O. Mandel, and I. Bloch, New J. Phys. **8**, 152 (2006).

[15] M. Greiner, O. Mandel, T. W. Hänsch, and I. Bloch, Nature **419**, 5154 (2002).

[16] J. Sebby-Strabley, B. L. Brown, M. Anderlini, P. J. Lee, W. D. Phillips, J. V. Porto, and P. R. Johnson, Phys. Rev. Lett. **98**, 200405 (2007).

[17] S. Will, T. Best, U. Schneider, L. Hackermuller, D. Luhmann, and I. Bloch, Nature **465**, 197 (2010).

[18] E. Toth, A. M. Rey, and P. B. Blakie, Phys. Rev. A **78**, 013627 (2008).

[19] P. R. Johnson, E. Tiesinga, J. V. Porto, and C. J. Williams, New J. Phys. **11**, 093022 (2009).

[20] J. Schachenmayer, A. J. Daley, and P. Zoller, arxiv 1101.2385 (2011).

[21] K. Sheshadri, H. R. Krishnamurthy, R. Pandit, and T. V. Ramakrishnan, Europhys. Lett. **22**, 257 (1993).

[22] D. van Oosten, P. van der Straten, and H. T. C. Stoof, Phys. Rev. A **63**, 053601 (2001).

[23] J. K. Freericks and H. Monien, Europhys. Lett. **26**, 545 (1994).

[24] K. Huang and C. N. Yang, Phys. Rev. **105**, 767 (1957).

[25] C. Chin, R. Grimm, P. Julienne, and E. Tiesinga, Rev. Mod. Phys. **82**, 1225 (2010).

[26] F. A. Wolf, I. Hen, and M. Rigol, Phys. Rev. A **82**, 043601 (2010).

[27] I. E. Mazets and J. Schmiedmayer, New J. Phys. **12**, 055023 (2010).

[28] E. Braaten and H.-W. Hammer, Ann. Phys. **322**, 120 (2007).

[29] T. Busch, B. Englert, K. Rzążewski, and M. Wilkens, Found. of Phys. **28**, 549 (1998).